Effects of ammonia addition on soot formation in co-flow diffusion flames

using laser-induced incandescence

Douwe Haringa, BSc

S2715678
EES-2022-591

Master Programme Energy and Environmental Sciences, University of Groningen

university of groningen / faculty of science and engineering / energy and sustainability research institute groningen

Effects of ammonia addition on soot formation in co-flow diffusion flames using laser-induced incandescence

Research report of
Douwe Haringa, BSc

July 2022

In partial fulfilment of the requirements for the degree of
Master of Science in Energy and Environmental Sciences

Report: EES-2022-591

Supervised by:

dr. A.V. (Tolja) Mokhov

Prof. dr. U. (Uli) Dusek

drs. S.S.A (Stijn) van Rijn

University of Groningen - Faculty of Science and Engineering
Energy and Sustainability Research Institute Groningen (ESRIG)
Energy Conversion (EC) and Centre for Isotope Research (CIO)

Nijenborgh 6
9747 AG Groningen
T: 050 - 363 4760
W: www.rug.nl/research/esrig

ACKNOWLEDGEMENTS

I would like to thank Tolja for the supervision and making this research possible. Being able to work in the lab and in the student room, especially with the company of other students also working on their thesis, was a welcome change after the pandemic. I am very grateful for the support of Stijn with his excellent daily supervision. His help in the lab and with the analysis of the data, as well as the great conversations during coffee breaks on topics ranging from politics to dinosaurs, made doing this research a pleasure. Thanks Stijn!

TABLE OF CONTENTS

SUMMARY

Energy production needs to be decarbonized in order to tackle climate change. Contributing to this can be the introduction of clean fuels, which do not emit carbon dioxide when combusted. A potential clean fuel can be hydrogen gas, however storage and logistics remain a hurdle for implementation. Ammonia is a hydrogen carrier with an existing infrastructure due to the incumbent Haber-Bosch process, and can be used as a clean, carbon-free combustion fuel. However, its combustion is challenging, as the properties of ammonia are less favourable for combustion compared to fossil fuels. As an intermediate step, ammonia can be added to regular carbonaceous fuels to reduce emissions and to gain more insight and experience with ammonia combustion.

This research focussed on the effect of ammonia addition on soot formation in flames from carbonaceous fuels. Soot formation along the flame centreline was measured using the laser-induced incandescence technique. To quantify the soot volume fraction in the flames of interest, a calibration was performed by laser light extinction through a laminar premixed flat flame using a McKenna burner. Subsequently, axial profiles of methane and ethylene co-flow laminar diffusion flames doped with ammonia and nitrogen were measured. Doping with nitrogen and ammonia was chosen to distinguish the physical and chemical effects, as nitrogen is inert. Soot suppressing effects were found in the doped methane flames, but not the doped ethylene flames.

SAMENVATTING

Om klimaatverandering tegen te gaan moet de energieproductie stoppen met het uitstoten van koolstof. Schone brandstoffen, die geen koolstof bevatten, kunnen hieraan bijdragen. Een potentiële schone brandstof is waterstof, maar de opslag het vervoeren van dit gas is maakt het lastig om dit te implementeren. Ammoniak is een waterstofdrager met een al bestaande infrastructuur omdat het al op grote schaal wordt geproduceerd via het Haber-Bosch proces. Echter, de verbranding van ammoniak is een uitdaging, omdat de chemische- en fysische eigenschappen van ammoniak minder gunstig zijn voor verbranding vergeleken met fossiele brandstoffen. Als tussenstap kan ammoniak worden toegevoegd aan reguliere brandstoffen om zo mogelijk de uitstoot te verminderen. Inzicht en ervaring met ammoniak verbranding wordt verkregen door deze tussenstap te gebruiken om zo te werken aan het gebruiken van ammoniak als schone brandstof.
Dit onderzoek richt zich op het effect op roetformatie in vlammen met toegevoegd ammoniak. Roetvorming in de vlam werd gemeten met behulp van de laser-geïnduceerde gloeitechniek. Om de roetvolumefractie in de vlammen te kwantificeren, werd een kalibratie uitgevoerd met de laserlichtuitdoving techniek door een laminaire, voorgemengde, platte vlam gemaakt met een McKenna-brander. Vervolgens werden axiale profielen van laminaire diffusievlammen van methaan en ethyleen met toegevoegd ammoniak of stikstof gemeten. Er is gekozen voor doping met of inert stikstof, of ammoniak om de fysische en chemische effecten te onderscheiden. Ammoniak en stikstof onderdrukte roetformatie in vlammen van methaan, maar niet in vlammen van ethyleen.

LIST OF ABBREVIATIONS

ADC	Analog-to-digital converter
BC	Black carbon
EC	Elemental carbon
HAB	Height above burner
HACA	Hydrogen abstraction-acetylene addition
LIF	Laser-induced fluorescence
LII	Laser-induced incandescence
LLE	Laser light extinction
OC	Organic carbon
PAH	Polycyclic aromatic hydrocarbons
PMT	Photo-multiplier tube
SVF	Soot volume fraction
TEM	Transmission electron microscopy

LIST OF FIGURES

1. INTRODUCTION

Anthropogenic activities including the emission of greenhouse gasses and particulate matter by the burning of fossil fuels result in a change in our planet's climate (IPCC, 2013). One of the effects of climate change is global warming. The Paris Agreement of 2015 (UNFCCC, 2015) sets the goal to limit the increase of global average temperature to 2°C with efforts to keep it below 1.5°C. A significant change in our energy system is needed to accomplish this, as most of our global energy production and generation is still based on fossil fuel combustion. Electrification is being pursued to utilize the clean electric energy being produced by renewable energy sources such as wind and solar energy. However, not all energy demanding applications can be electrified easily. Remote locations do not necessarily have an electrical energy network which is needed to deliver and use electrical energy. Furthermore, electrical energy storage is still a challenge, especially on larger scales. Our current energy system is based on the readily available chemical energy in the form of a combustible fuel. Therefore, there is a demand for an (chemical) energy vector that has similar properties as incumbent combustible fossil fuels, such as easy storage, transportation and useful for dispatchable generation.

Hydrogen is often proposed as a fossil free clean energy vector for use in fuel cells or combustion as it can be produced in a renewable way by electrolysis using wind or solar power. However, in gaseous form its volumetric energy density is very low. Being the smallest and lightest molecule, liquefying or compression hydrogen to obtain usable volumetric energy densities is difficult due to its unfavourable thermal properties. The boiling point of hydrogen is -253°C and pressurized storage needs pressures ranging between 300 and 700 bar (Amos, 1998). Reaching and maintaining these extreme temperatures and pressures is done by energy intensive processes, reducing the functionality of hydrogen as energy vector.

In order to improve storage, transportation and handling, we can look for an energy vector which can carry the so-called green hydrogen produced by electrolysis with electricity from renewable energy sources. A suitable, carbon free, hydrogen- and energy carrier is ammonia (NH3). Ammonia can be produced from nitrogen and green hydrogen (Rouwenhorst et al., 2020) using the well-established Haber-Bosch process, which has been in operation for over a century (Appl, 2011). Ammonia is mostly used as a fertilizer for crops, enabling the Green Revolution, and is therefore produced in enormous amounts on global scale. This has led to the development of efficient, and technologically mature, ammonia storage and transportation infrastructure, which is already in place today.

Ammonia can be used in solid oxide fuel cells (Wang, B. et al., 2022), but can also be combusted. However, its combustion is difficult, as its laminar burning velocity is relatively low and its ignition temperature relatively high. Furthermore, its heating value and flame temperature are also low compared to hydrogen and comparable hydrocarbon as shown in table 1 from Kobayashi et al. (2019).

Table 1-1. Thermal properties and fundamental combustion characteristics of ammonia and hydrocarbon fuels.

Fuel	**NH_3**	**H_2**	**CH_4**	**C_3H_8**
Boiling temperature 1 atm (°C)	-33,4	-253	-161	-42,1
Condensation pressure at 25 °C (atm)	9,90	N/A	N/A	N/A
Lower heating value (MJ/kg)	18,6	120	50,0	46,4
Flammability range (Φ)	0,63~1,40	0,10~7,10	0,50~1,70	0,51~2,50
Adiabatic flame temperature (°C)	1800	2110	1950	2000
Maximum laminar burning velocity (m/s)	0,07	2,91	0,37	0,43
Minimum auto ignition temperature (°C)	650	520	630	450

An additional challenge to ammonia combustion is NOx formation. However, it should be noted that NOx formation can be limited by ensuring conditions that lead to the full combustion of ammonia, given by reaction equation 1-1.

$$4NH_3 + 3O_2 \rightarrow 2N_2 + 5H_2O \qquad \textit{Equation 1-1}$$

These challenges made that ammonia was not used for combustion systems, as hydrocarbon fuels were preferred. The need for a carbon free energy source has renewed interest in ammonia as a combustible energy source, to which this research contributes.

Due to issues states above, an immediate switch from hydrocarbon fuels to ammonia as combustible energy source is not possible. More research in ammonia combustion is needed, and technological applications need to be adapted. In the meanwhile, an intermediate solution can be the co-firing of ammonia alongside hydrocarbon fuels. Co-combustion enables a possible reduction of emissions and gaining experience with ammonia combustion with relatively minimal effort. Mixing ammonia with hydrocarbon fuels will alter reaction pathways in the flame. This will affect which combustion products will be formed. In this thesis, the focus is on the effect of ammonia addition to carbonaceous fuels on soot formation. This will be studied by measuring soot volume fraction (SVF) in co-flow diffusion flames.

1.1 Research question and hypothesis

The main research question to be answered in this thesis is:

"What is the effect of co-combusting ammonia with carbonaceous fuels on flame soot formation?"

The carbonaceous fuels selected are methane, as it is the largest component of natural gas, and ethylene, as this is the standard fuel in flame sooting research. To complement the research question, the following sub question was stated:

"Does fuel type alter the effect of ammonia addition on soot formation, i.e. is there a difference in the effect between ethylene and methane flames?"

Based on recent literature, a survey is given in chapter 2 section 3, the following hypothesis is formulated:

"Co-combusting ammonia has a suppressive effect on flame soot formation in methane and ethylene flames."

In order to test the hypothesis, the following research activities were performed:

- Calibration of laser-induced incandescence setup using laser light extinction through a stabilized premixed laminar flat flame produced by a McKenna burner.
- Determining experimental conditions to be tested in methane and ethylene flames.
- Measuring axial profiles of methane and ethylene flame consisting of:
    - Pure fuel
    - Fuel + nitrogen addition
    - Fuel + ammonia addition

1.2 Outline of the report

The report will be structured in the following manner.
First, in chapter 2, the theoretical background of this thesis will be explained. The sections will cover the theory of combustion and soot formation, and an overview of the used optical measuring techniques. Chapter 2 is concluded with brief survey of the latest literature in the field. Chapter 3 describes the methodology used to conduct the experiments. A description of used equipment as well as an illustration of the overall setup is given and explained. The results are presented and discussed in chapter 4, from which conclusions will be drawn in chapter 5 to answer the research questions. The report is wrapped up with a recommendation for future research, after which consulted literature and appendices follow.

2. THEORETICAL BACKGROUND

In this chapter, we will explore some general theory about combustion and soot formation and the measuring techniques laser-induced incandescence and laser light extinction. Most of the information about combustion and soot formation is based on the book Combustion: Physical and Chemical Fundamentals, Modeling and Simulation, Experiments and Pollutant Formation (4th ed.) by J. Warnatz, U. Maas & R.W. Dibble (2006). The review of Michelsen et al. (2015) and chapter 9 in Applied Combustion Diagnostics by K. Kohse-Höinghaus & J. B. Jeffries (2002) provided most of the information on laser-induced incandescence and laser light extinction.

2.1 Combustion and soot formation

Combustion the oldest energy extracting technology of mankind. Still, most of the worldwide services and applications needing energy input (such as transport, power generation and heating), is provided through combustion. Therefore, studying and knowing the underlying processes is valuable for society. In order for combustion to take place, a fuel combined with an oxidizer (most often oxygen from air) need to be present and heated or ignited at a certain temperature. If neither fuel or oxidizer is present at the required amounts, combustion cannot take place or the process will stop.

We can characterize the composition of the fuel oxidizer mixture based on the ratio of fuel to oxidizer compared to the ratio of fuel to oxidizer in the stoichiometric reaction. A stoichiometric combustion reaction is a reaction in which the reactants consume each other completely to only form carbon dioxide and water. This is what is called the (fuel) equivalence ratio, commonly denoted by the Greek letter phi (Φ) and is defined by equation 2-1 in which n represents the number of moles of fuel or oxidizer in the actual and stoichiometric reactions:

$$\Phi = \frac{n_{fuel}/n_{ox}}{n_{fuel,stoi}/n_{ox,stoi}} \qquad \textit{Equation 2-1}$$

It can be seen from this equation that at an equivalence ratio $\Phi = 1$, the ratio fuel to oxidizer is the same as in the stoichiometric reaction and thus the combustion is said to be stoichiometric. At $\Phi > 1$, there is an excess of fuel, and at $\Phi < 1$ there is excess oxidizer. $\Phi > 1$ is called a rich combustion, while $\Phi < 1$ is called a lean combustion.

Another important combustion parameter is the maximum laminar burning velocity v_L (m/s). Burning velocity depends on mixture composition, pressure and initial temperature. This is an important characteristic, as the burning velocity should be greater or equal to the exit velocity v_e (m/s) of gasses that are to be combusted. If this is not the case, the flame will be blown off.
Exit velocity is also used in the calculation of the exit Reynolds number. Reynolds number indicates if a flow is in the laminar or turbulent regime. A Reynolds number < *2300* indicates laminar flow in which inertial forces are dominant, while a Reynolds number > *4000* indicates turbulent flow in which viscous forces are dominant (Engineering Toolbox, 2003). Flows with Reynolds numbers in between these values are in the transition or transient region and are neither fully laminar or turbulent. Reynolds numbers are calculated by equation 2-2 (Mahmoud et al., 2018).

$$Re = \frac{\rho v_e L}{\mu} \qquad \textit{Equation 2-2}$$

In equation 2-1, ρ is the exit fuel density (kg/m3), v_e is exit velocity (m/s), L is the characteristic length (m) which is a matter of convention and often taken to be a diameter of the flow, and μ is the viscosity (kg/(m·s)).

Before we can distinguish different flame types, we need to know if the fuel and oxidizer were premixed or not. In premixed flames, the fuel and oxidizer are mixed before ignition, while in non-premixed flames this is not the case. Diffusion flames, in which the fuel and oxidizer mix via diffusion are per definition non-premixed. In these flames, a radial distribution of Φ can be given with $\Phi \approx 0$ at the flame edges and $\Phi \approx \infty$ at flame centreline.
Examples of the different flame types based on fuel/oxidizer mixing, fluid motion and fuel equivalence ratio are given in figure 2-1.

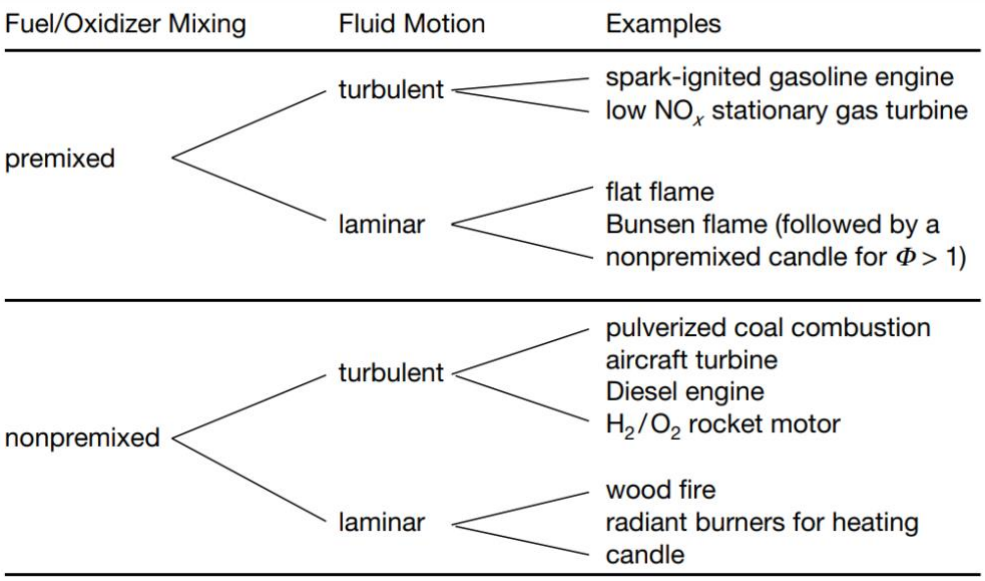

Figure 2-1. Examples of combustion systems based on reactant mixing and flow type.
Figure from Warnatz, U. Maas & R.W. Dibble (2006).

In this research, the focus in on soot formation in laminar co-flow diffusion flames. Soot is the carbonaceous product of incomplete combustion. This occurs in fuel rich circumstances, as not all fuel has the opportunity to fully oxidize to carbon dioxide (Warnatz et al., 2006). Soot consists mainly of various polycyclic aromatic hydrocarbon (PAH) products and complexes of which the different components are classified based on the method of detection.

If soot is classified based on optical absorption, different classes are distinguished. Black carbon (BC) absorbs all light, while organic carbon (OC) consists of molecules that do not absorb across the whole spectrum. If different soot constituents are classified based their thermal properties and volatility, the volatile fraction is called organic carbon (OC) and the inert fraction is called elemental carbon (EC) (Pöschl, 2005). BC and EC are very similar, but the formal difference in definition is based on the method of classification.

Research in the field of soot and BC emissions is important, as BC is estimated to be the most important aerosol radiative forcer. Of all radiative forcing components, only carbon dioxide and methane have a greater positive effect as shown in figure 2-2. Furthermore, aerosols derived from soot and BC are dangerous for human health (Kennedy, 2007).

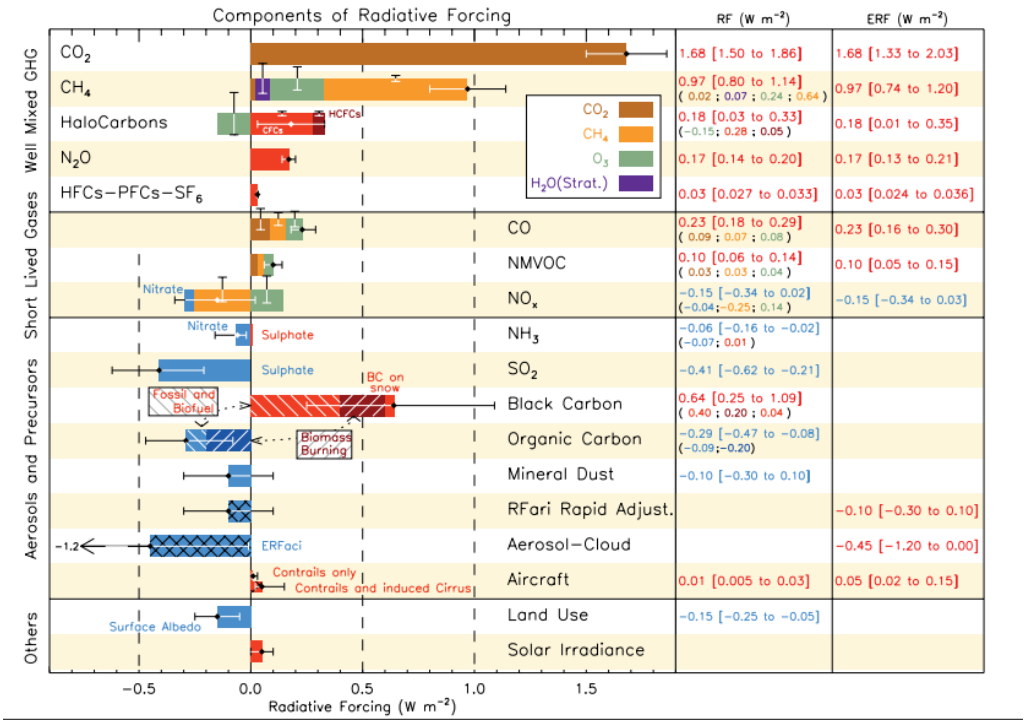

Figure 2-2. Components of radiative forcing.
Figure from the 2013 IPCC report: Climate Change 2013: The Physical Science Basis.

As shown in equation 1-1, a combustion reaction can be described by the reaction equation between the fuel and the oxidizer, giving the resulting combustion products. Another example is the reaction equation of the stoichiometric combustion of methane with oxygen, given below in equation 2-3.

$$CH_4 + 2O_2 \rightarrow 2H_2O + CO_2 \qquad \textit{Equation 2-3}$$

However, this does not fully encompass the complex reaction that take place during the combustion process. Figure 2-2 shows the reaction pathways of the fuel-rich combustion of methane.

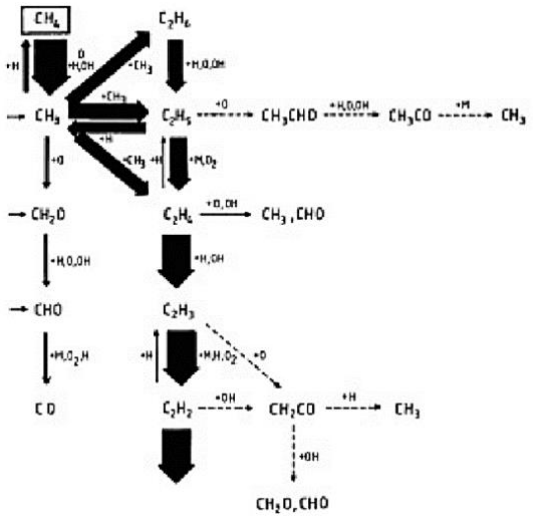

Figure 2-3. Reaction flow of rich methane combustion.
Figure from Warnatz, U. Maas & R.W. Dibble (2006).

As can be seen in figure 2-3, different species are generated and consumed during the combustion process. One of the major pathways is towards acetylene (ethyne) formation, which is an important precursor to soot formation. The reaction pathways shown are is for combustion of pure methane, which is the most simple and small hydrocarbon there is. If the combusted fuel is a higher alkane, alkene or a mixture of hydrocarbons, possibly containing additives, a much larger amount of possible reactions can take place. This leads to an increasing complex network of reaction flows, which is often not yet fully understood.

As mentioned before, soot mainly consist of PAHs which form a graphene like structures with morphologies and C/H ratios depending on the fuel mixture and formation conditions (Xi et al., 2021). The smallest PAH is benzene, which can be formed by trimerization of three acetylene molecules (Havenith et al., 2003) according to figure 2-4.

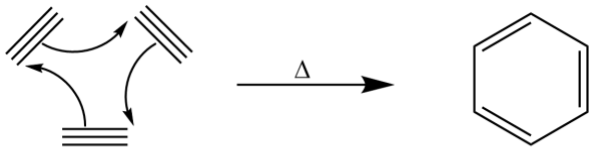

Figure 2-4. Trimerization of acetylene to benzene (figure made using ChemDraw).

Benzene can subsequently grow to larger PAHs by annulation, condensation, or hydrogen abstraction-acetylene addition (HACA) (Pejpichestakul et al., 2019) until particle sizes are reached. These soot formation processes in a flame over time (increasing axial positions) are shown in figure 2-5.

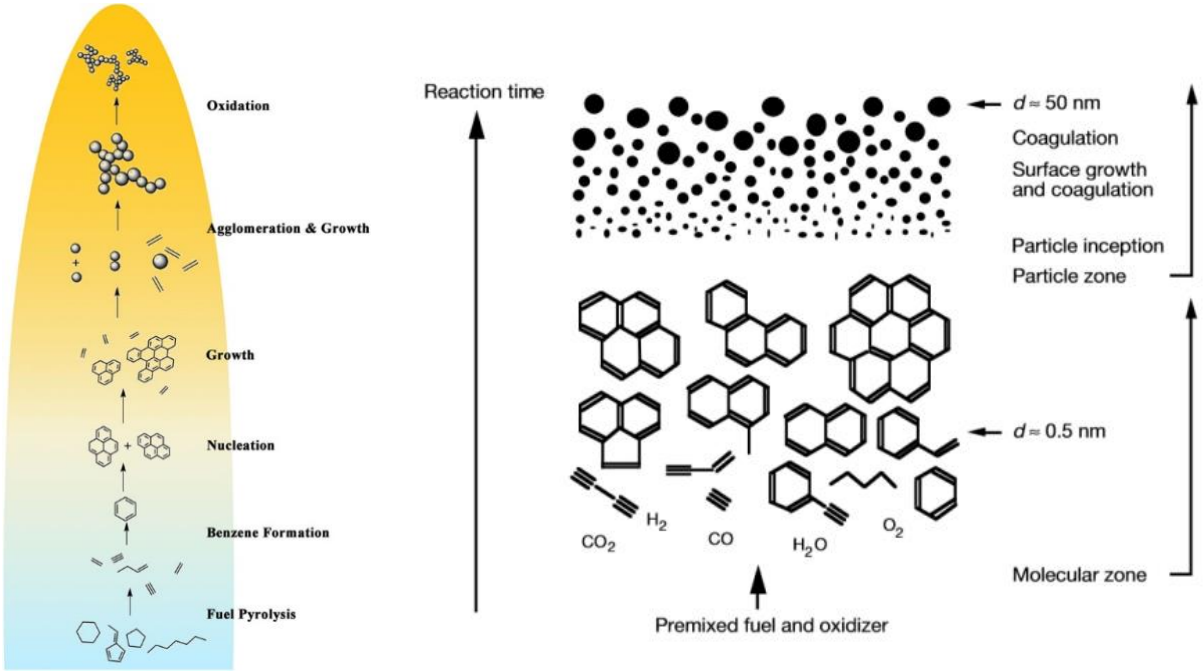

Figure 2-5. Physical and chemical processes of soot formation.
Left figure from Xi et al. (2021), right figure from Warnatz, U. Maas & R.W. Dibble (2006).

2.2 Laser-induced incandescence

Laser-induced incandescence, abbreviated to LII, is an optical diagnostic method which can be used to perform in-situ measurements of the soot volume fraction (SVF) in a flame. Interest in LII as application for soot measurements was sparked due to interference with Raman diagnostics in soothing combustions (Santoro & Shaddix, 2002). Mature soot, consisting mostly of BC, absorbs strongly in across wavelengths ranging from infrared to ultraviolet and has a sublimation point around 4000 K (Michelsen et al., 2015). Due to this absorption, the soot particles heat up and start to emit quasi-black body radiation. LII signal is derived from this radiative emission, as it can be collected using a photo-multiplier tube (PMT). Apart from this radiation, other processes occur when soot is irradiated, as shown in figure 2-6.

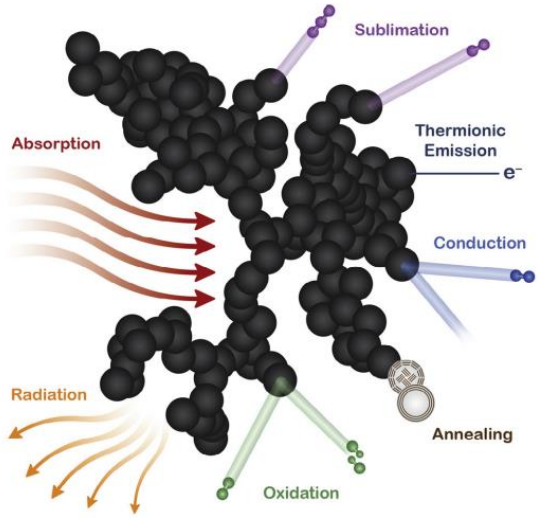

Figure 2-6. Heating and cooling processes during LII signal collection.
Figure from Michelsen et al. (2015)

The most important processes for LII are the initial heating due to absorption, and cooling due to radiation. Therefore, we will further elaborate on their mechanisms.
In the Rayleigh regime, with the diameter of the particle being significantly smaller than the wavelength of the laser, the absorptive-heating rate Q_{abs} can be calculated by multiplying the absorption cross section σ_{abs} of the particle times the time dependent irradiance of the incident laser $E_e(t)$. This is formulated by equation 2-4 (Michelsen et al., 2015).

$$Q_{abs} = \sigma_{abs} E_e(t) = \frac{\pi^2 d_p^3 E(m)}{\lambda_L} E_e(t) \qquad \textit{Equation 2-4}$$

In equation 2-4, d_p is the particle diameter, $E(m)$ is the refractive index function for absorption, and λ_L is laser wavelength. From equation 2-4, it can be seen that the absorption cross section for small particles in the Rayleigh regime scale with particle volume. If all particles reach the maximum signal at the same peak temperature (i.e., the sublimation point), the peak signal will scale with the volume of the particle.

$$\varepsilon_\lambda = \frac{4\pi d_p E(m)}{\lambda} \qquad \textit{Equation 2-5}$$

The radiative cooling rate Q_{rad} can be calculated by integrating the Planck function, modified by ε_λ (equation 2-5) to account for deviations from a perfect black body, over all wavelengths, resulting in equation 2-6.

$$Q_{rad} = -8\Gamma(5)\zeta(5)\frac{\pi^3 d_p^3 (k_B T^5 E(m)}{h(hc)^3} \qquad \textit{Equation 2-6}$$

In equation 2-6, Γ and ζ indicate the respective gamma function and Riemann zeta function of *5*, evaluating to *24* and *1,0363*. For a more thorough derivation and the mathematical descriptions of the other processes shown in figure 2-6, the reader is referred to Michelsen et al. (2015).
It can be seen that in both absorption and radiative emission, the refractive index function *E(m)* is important. This parameter is also important when calibrating LII signals for SVF, as the calibration is only valid if the value of *E(m)* is the same for the calibration by LLE as for LII-measurement conditions. It is defined by equation 2-7.

$$E(m) = -Im\left\{\frac{m^2-1}{m^2+2}\right\} \qquad \textit{Equation 2-7}$$

In equation 2-7, *m* is the complex index of refraction, given by $m = n - ik$. In this expression, the real part *n* is the refractive index and indicates phase velocity, while the imaginary part *k* indicates the extinction or attenuation of the wave propagating through the material (Hecht, 2002). Often, the value of $m = 1{,}57 - 0{,}56i$ is used (Smyth & Shaddix, 1996), resulting in $E(m) =$ 0,26.

To calibrate the LII signal, LLE is used. This is a line of sight technique, based on the Beer-Lambert-Bouguer law, and compares the incident light intensity I_0 with the intensity of the light transmitted I_T through the system of length l (equation 2-8).

$$I_T = I_0 e^{-\tau_{ext} l} \qquad \textit{Equation 2-8}$$

The amount of extinction is given by the turbidity of extinction τ_{ext} and is related to both the absorption and scattering cross section (Langenkamp, 2018). With the fair assumption for soot particles that the absorption cross section is larger than the scattering cross section, the turbidity can be approximated by equation 2-9 (Sorensen, 2001).

$$\tau_{ext} \approx nN\sigma_{abs} = nN4\pi k a^3 E(m) \qquad \textit{Equation 2-9}$$

In equation 2-9, *n* is the number density of soot aggregates, *N* is the number of monomers (or primary particles) in the aggregate, *k* is the wave number and *a* is the radius of the monomers that constitute the aggregate. Since the volume of a sphere can be given by $V = 4\pi a3/3$, the volume fraction of soot can be expressed by equation 2-10. For a more detailed derivation, the reader is referred to literature (Sorensen, 2001) and (Langenkamp, 2018).

$$f_v = nN\frac{4\pi a^3}{3} = \frac{\tau_{ext}}{3kE(m)} \qquad \textit{Equation 2-10}$$

2.3 Literature survey

In 1981, Bockhorn et al. (1981) pioneered with determining soot concentration and particle sizes by measuring LLE and scattering in flat premixed laminar propane flames doped with ammonia or hydrogen. They reported a decrease in soot concentration and mean particle size with both additions, with ammonia having the greater effect.
After a dry spell, lately a renewed interest in the topic of ammonia combustion and its effect on soot formation is sparked due to the need for clean fuels to combat climate change. Several papers have been published recently, investigated this topic using similar or complementary approaches compared to this study. To get a sense of the recent progress, consensus and disagreements in this field, an overview of a select number of papers will be given in this section in a chronological order.

Valera-Medina et al. (2018) wrote a review on ammonia for power. Apart from some general information about ammonia, extracting energy out of ammonia is described using fuel cell and combustion technologies on both fundamental and technological levels. It was concluded that once ammonia combustion is understood better, it has the potential of operating at high power levels with tolerable emission levels.

Kobayashi et al. (2019) reviewed the science and technology of ammonia combustion. An overview is given on challenges related to ammonia combustion such as its low flammability and NOx emissions. They begin with stating the properties of ammonia and how it compares to other fuels such as hydrogen and methane. Then, fundamental characteristics of ammonia flames are described and compared to those of methane. This is followed by an investigation of chemical kinetics of ammonia oxidation and emission abatement in an ammonia fuelled gas-turbine combustor.

Wang, Y. & Chung (2019) provide a very extensive review on soot formation studies in counterflow flames. First, soot formation pathways, nucleation, growth and oxidation are discussed. Secondly, experimental techniques for soot related measurements are explored. At last, sooting in counterflow flames is discussed in more detail. A summary is given of soot studies performed in counterflow flames detailing the fuel, topic and methods. Furthermore, the effects of fuel type, dilution and additives, pressure, temperature, strain rate and other variables on soot formation are described.

Bennet et al. (2020) measured SVF in counterflow ethylene flames with ammonia addition by planar LII and found that ammonia reduced SVF by 4-6% per 1% ammonia addition. Experiments were simulated and it was found that no significant effect on temperature was produced by ammonia addition, ruling out temperature effects on soot suppression. PAH's were measured by planar LIF and gas samples were taken and passed through a gas chromatographer / mass spectrometer. It was concluded that ammonia did have a chemical effect in reducing soot formation, and this effect began to appear with PAHs larger than 2 to 3 rings.

Montgomery et al. (2021) experimentally investigated soot volume fractions by colour-ratio pyrometry and mole fractions of gas-phase species by on-line electron impact mass spectrometry of methane co-flow diffusion flames with up to 40v% ammonia. This was complemented by computer simulations. Results were compared to flames with added nitrogen to separate thermal and dilution effects from chemical effects. A suppressive effect was found on soot volume fraction in both the ammonia and nitrogen doped flames, with ammonia addition having a greater effect. The model did approach the effect of nitrogen addition, but was inaccurate in predicting the effect of ammonia addition. Similar results and differences were found in the mole fractions of C_2H_2 and C_6H_6 in ammonia and nitrogen doped flames. Therefore, it was concluded that ammonia addition has a strong chemical effect relative to nitrogen in methane flames on suppressing soot volume fraction and formation of C_2H_2 and C_6H_6. The disagreement in the model is due to the lack of understanding in chemical combustion pathways of ammonia/methane mixtures.

Boyette et al. (2021) studied turbulent non-premixed jet flames of ethylene/nitrogen substituting nitrogen for ammonia and/or hydrogen. Axial profiles of soot formation were measured using LIF and LII. It was found that hydrogen substitution increased soot formation, while ammonia substitution decreased soot formation. Apart from soot measurements, LIF-OH, LIF-CH and signal decay time constants were measured.

Liu et al. (2021) measured spatial distributions of soot volume fraction, polycyclic aromatic hydrocarbons and OH radicals by two-colour LII and planar LIF in laminar ethylene diffusion flames with ammonia addition with up to 60% by mole fraction. Temperature profile along the centreline was obtained by rapid thermocouple insertion technique and primary particle sizes were measured by TEM. In order to better understand the underlying cause of the effect of ammonia addition, chemical kinetic analysis of the flames was performed numerically. Increasing ammonia doping concentration increased flame height and decreased temperature at the same height. PAH formation, soot nucleation and surface growth were inhibited by NH_3 addition, reducing total soot load. Primary particle size also decreased with ammonia addition.

Zhu et al. (2021) shot chemiluminescence spectra of ammonia-methane-air laminar premixed twin-flames to measure intensities of $NO*$, $OH*$, $NH*$, $CN*$, CO_2*, and $CH*$ excited radicals at varying equivalence ratios, ammonia fractions and strain rates. A database for model validation was created and various chemiluminescence intensity ratios were suggested as surrogates for equivalence ratio and/or ammonia fuel fraction.

Steinmetz et al. (2022) substituted or added ammonia or hydrogen to laminar co-flow flames using ethylene or methane. LII was used to measure SVF and was complemented with LIF measurements to estimate particle size and combined with a chemical kinetic analysis. It was found that ammonia inhibits soot formation in both methane and ethylene flames, and hydrogen enhances soot formation in both methane and ethylene flames.

Shao et al. (2022) presents particle size distributions and chemical compositions of soot using a Scanning Mobility Particle Sizer and a Fourier-Transform Ion Cyclotron Resonance Mass Spectrometer in a laminar premixed ethylene flame doped with ammonia. Temperatures of the investigated flames were nearly identical, suggesting the differences in soot formation to be of chemical nature. Results showed that PAHs were the main components, while nitrogen containing PAHs did not contribute significantly to soot formation processes. Chemical kinetic analysis showed that generation of C-N species removed carbon from soot precursor formation, thus reducing total soot.

Ren et al. (2022) researched the effects of ammonia addition on PAHs and soot formation in ethylene co-flow diffusion flames using planar LII, planar LIF, thermophoretic sampling particle diagnostic method combined with TEM. Flame temperature was measured using the rapid insertion thermocouple technique and a chemical kinetic analysis was performed. The results of both planer LII, planar LIF and TEM imaging revealed that ammonia addition supresses PAH and soot formation and change its distribution, morphology and formation zone.

3. EXPERIMENTAL APPROACH

A Spectra-Physics Quanta-Ray GCR-150 pulsed Nd:YAG laser was operated at 1064 nm with a frequency of 25 Hz, a pulse width of 8 ns and carrying 70 mJ per pulse. The beam was passed through an attenuator to reach a laser power level varying between 0,3 and 0,6 watt. LII signal was found to be independent of laser power, as at high fluences all soot is sublimed leading to negligible attenuation throughout the sample (Michelsen et al., 2015). The laser beam is focussed above the burner by a 500 mm focal length lens to increase the resolution of the spatial measurements. The signal is detected and amplified using a PMT (EMI 9558B) and measured by a 54830 series Infinium Oscilloscope. Data acquisition from the PMT was in phase with the laser pulses by connecting the oscilloscope with the laser pulse generator to increase signal to noise ratio. For LII calibration, LLE was measured using a separate laser (Coherent Sapphire 100 mW continuous wave laser) operating at 532 nm. Measuring and/or regulating fuel supply, Bronkhorst® EL-FLOW® Thermal Mass Flow Meters/Controllers were used. All analogue signals were converted to digital signals via an analogue to digital converter (ADC). All data was processed on a computer using home-made software written in Python. A schematic overview of the setup is given in figure 3-1.

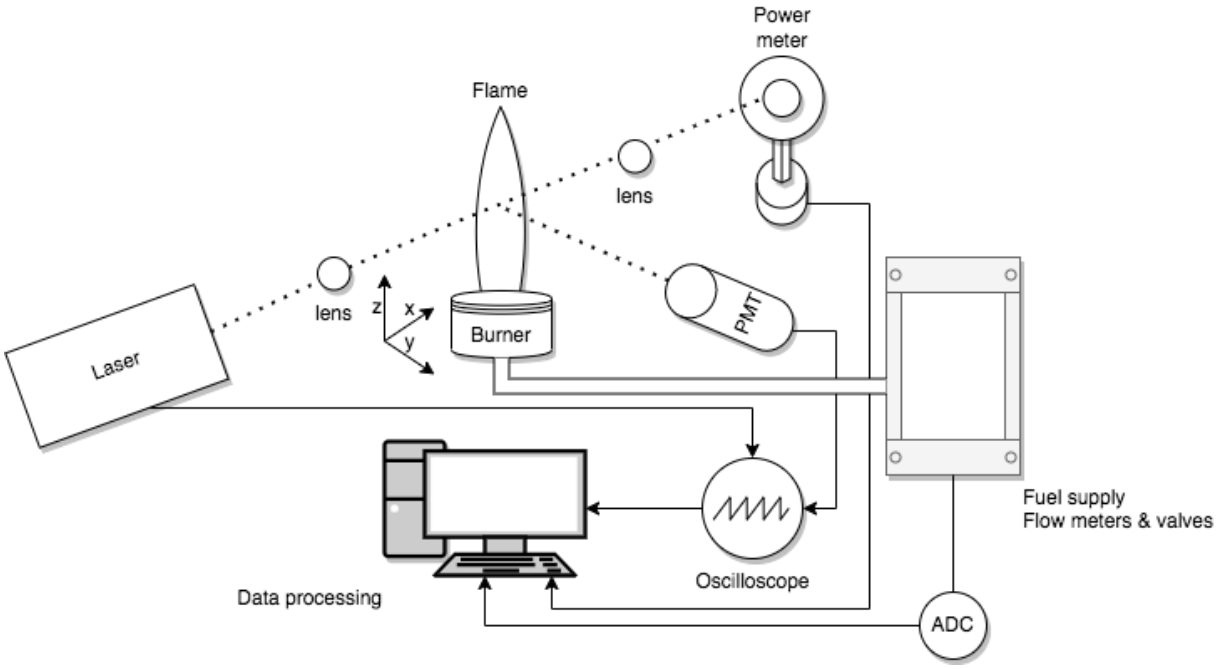

Figure 3-1. Schematic overview of experimental setup (own work).

The interchangeable burner was placed on a Parker positioner system with a positioning uncertainty less than 0,1 mm. For the calibration by LLE, a McKenna burner (figure 3-2) was used to produce a flat premixed 1-D flame. Fuel (ethylene) and oxidizer (air) is mixed before being led to the burner inlet. The burner was water cooled and has a porous surface to ensure proper mixing and a homogeneous flame in the radial direction, with the only variation in the flame being in the axial direction. The flame is shielded from the environment by a surrounding flow of nitrogen creating a protective shroud. LII signals were measured along the path of the LLE laser, while measuring the extinction. Total LII signal was obtained by integrating the signal along the length of the system, corresponding to the total soot volume fraction present in this length. This was done for flames of varying equivalence ratios, and thus varying LII signal and soot volume fractions. A linear fit was made to determine the calibration factor for LII signal to SVF.

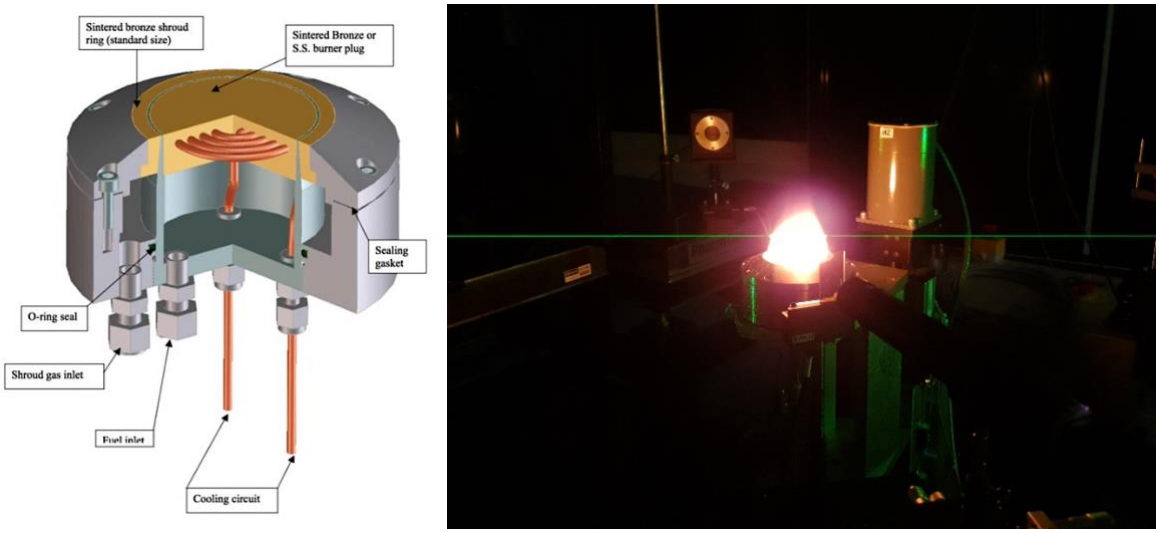

Figure 3-2. Details of McKenna burner (left) and a produced flat flame (right) with visible LLE laser. Figure (left) from www.flatflame.com/burner-description.html, accessed 10 July 2022, photo (right) from own work.

Soot measurements were made of co-flow diffusion flames from methane and ethylene. Axial profiles were measured of the pure flames, and with either ammonia or nitrogen addition. The flame was stabilized by the air co-flow having the same exit velocity as the fuel gasses and a quartz tube surrounding the burner setup (figure 3-3). The methane flame was taken as the reference flame, with a flow of 0,25 L/min resulting in an exit velocity of 13 cm/s. Switching to ethylene, either carbon flow or exit velocity was kept constant compared to the methane reference flame.

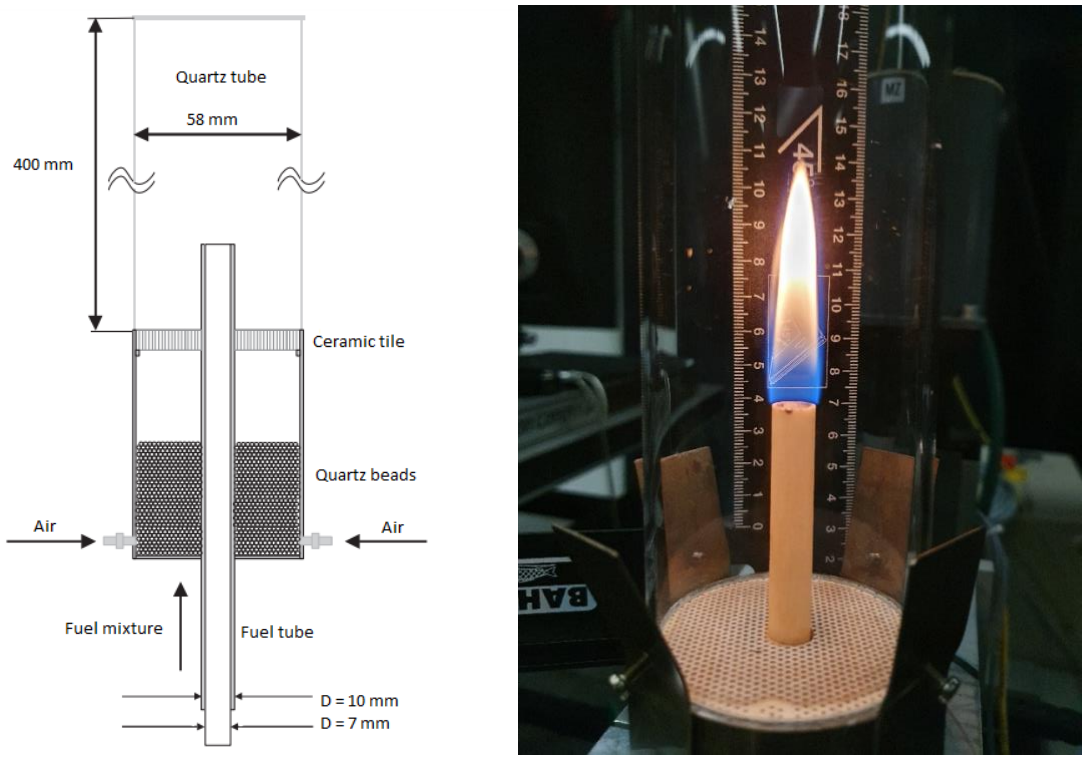

Figure 3-3. Details of diffusion burner (left) and a produced co-flow diffusion flame (right). Figure (left) adapted from A.V. Sepman et al. (2013), photo (right) from own work.

4. RESULTS AND DISCUSSION

In this section the results will be presented and discussed accordingly. We will start by giving the results of calibrating the LII setup with LLE through a horizontal flat flame. Then, the results of the methane flames are presented. At last, the ethylene flames are presented, discussed, and compared to the methane flames.

4.1 Calibration

An example of a horizontal (radial) profile through a flat flame produced by the McKenna burner is given in figure 4-1. Ethylene is used to obtain high enough sooting fractions that can be measured using LLE. Points 1 and 10 are outside of the flame where there is no soot present, and therefore no significant LII signal is observed.

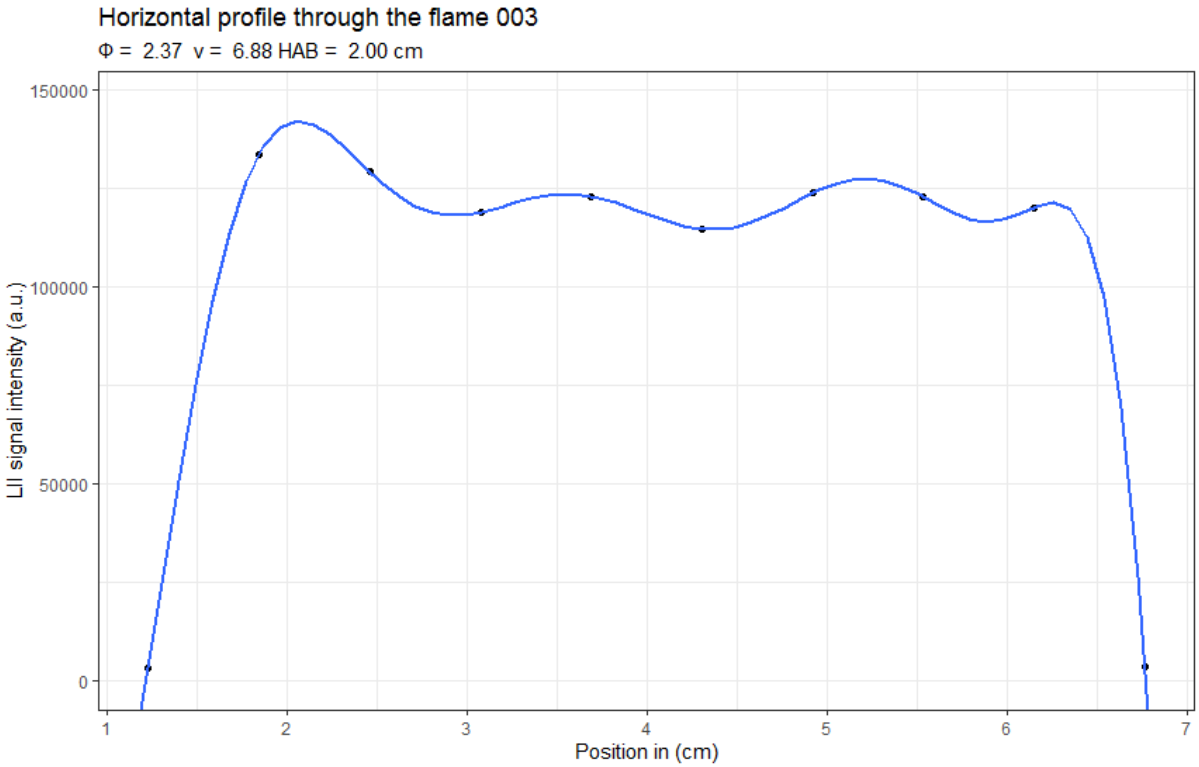

Figure 4-1. Radial profile LII signal through an ethylene flat flame produced by a McKenna burner.

Calculating the total LII signal by integrating along the profile and comparing this with the SVF calculated using the LLE technique results a LII intensity corresponding to the calculated SVF. Varying the equivalence ratios of the calibration flames, and therefore varying the SVF as a higher equivalence ratio leads to more soot, led to the following calibration curve (figure 4-2) from which the conversion factor to SVF was calculated.

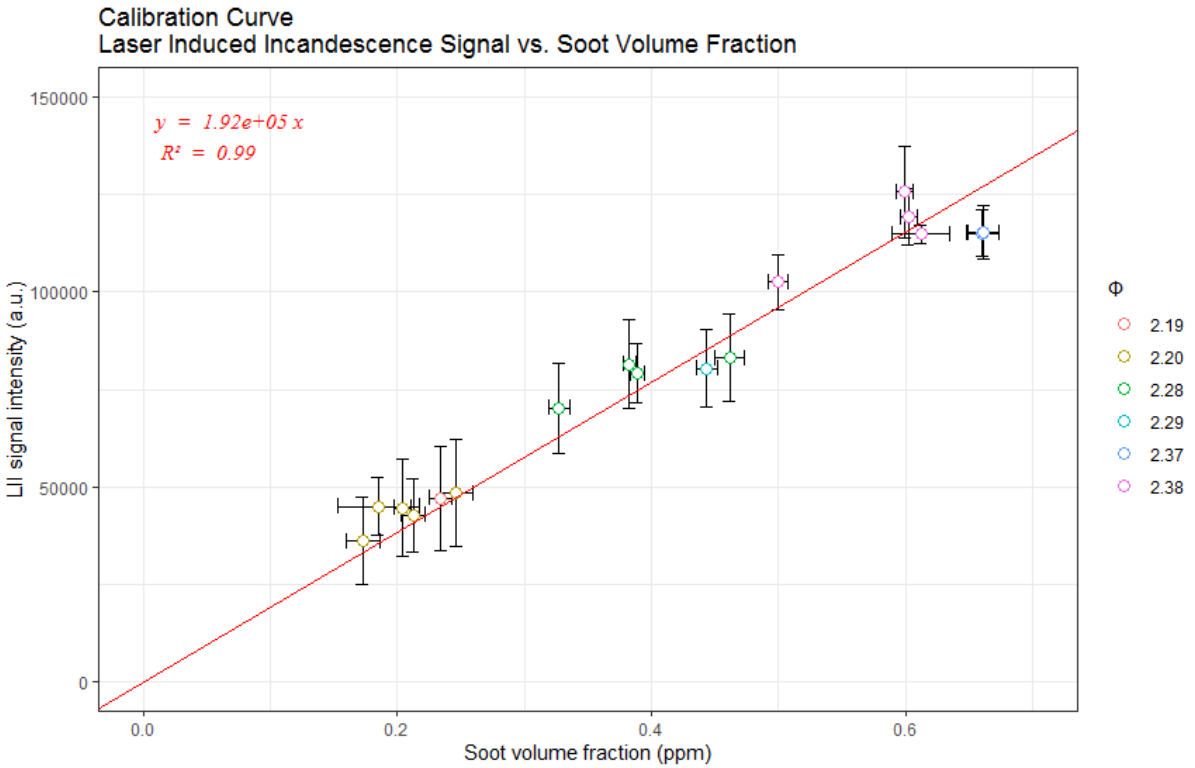

Figure 4-2. Calibration curve of the measuring setup for LII intensity to SVF.

From the calibration curve, it can be seen that a small change in equivalence ratio can have a significant effect on SVF and thus on LII signal intensity. Ethylene was used as it is the standard fuel in soothing combustion research. Highly soothing flames can be produced at relatively low equivalence ratios, which is beneficial for flame stabilization. The calibration points are in a similar SVF range as the methane flame of interest, increasing the accuracy of the calibration. However, for the ethylene diffusion flames, SVF is higher by an order of magnitude. To improve the calibration, the curve should be extended taking higher SVF into account. However, if fluence curves are similar in the zones of interest, a fixed proportionality factor between LII signal and SVF can be assumed (Michelsen et al., 2015).

4.2 Methane

First, methane co-flow diffusion flames were investigated. To assess variability in LII signal, runs were performed *in duplo*. It can be seen from figure 8-1 that the shot vertical (axial) profile along the flame centreline is consistent. Subsequently, nitrogen and ammonia were added to the flame in respectively 18v% and 17v% compared to methane flow (figure 8-2). Flame length was approximately 7 cm and did not change between the two additions. Nitrogen is inert, and will therefor only have physical effects on suppression SVF in by flame dilution and cooling. Ammonia is combustible, and actively alters the combustion pathways, leading to a chemical effect on soot suppression. Both effects and their relative contribution are visualized in figure 4-3.

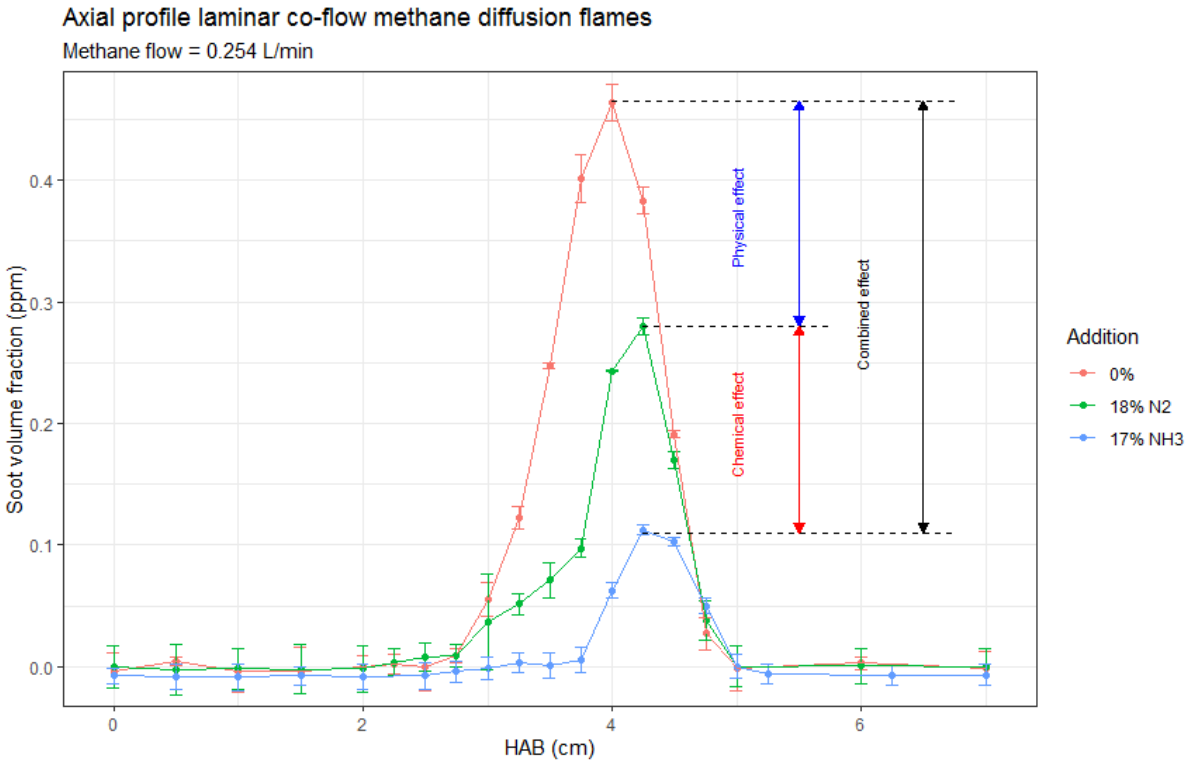

Figure 4-3. Suppressive effects on soot formation of nitrogen and ammonia addition in methane co-flow diffusion flames.

Apart from the reduction in SVF, the peak is shifted to higher HAB due to flame lift off. This is in accordance with literature (Steinmetz et al., 2022) and can be explained due to the increase in flow due to addition and lower burning velocity of ammonia. Due to time constraints, no radial profiles at varying HAB were shot during this research. Therefore, total (volume-integrate) effects on soot formation suppression cannot be calculated. However, suppressive effects are expected to behave similarly in radial measurements, and thus the suppressive effect in peak SVF along the centreline is indicative for overall soot suppression in the flame (Boyette et al., 2021). To further investigate the suppressive effect on soot formation, this experiment can be repeated varying the volumetric percentage added of both nitrogen and ammonia.

4.3 Ethylene

For the comparison of ethylene to methane, either flow rates and thus exit velocity or carbon flow was kept constant compared to the methane flames. Keeping the flow rate at 0,25 L/min, significantly increased the flame height (figure 8-3) This resulted in a highly sooting flame which could not be fully measured along the centreline due to limited range of the positioner. An interesting observation is the decrease in SVF at a HAB of 5 cm, after which the SVF rises again until the limit of the positioner is reached as shown in figure 4-4. HAB 5cm corresponds with the brightest spot in the flame. As no measurements on temperature or particle size distribution were done, it cannot be said if this decrease is due to a measuring artefact or due to other effects which are not yet understood. The decrease is consistent across both nitrogen and ammonia addition. Addition does not seem to suppress soot formation in a significant manner. This is contradicting to the results found by Ren et al. (2022). However, different flame characteristics and conditions were used as they used much larger doping concentrations and lower fuel flows.

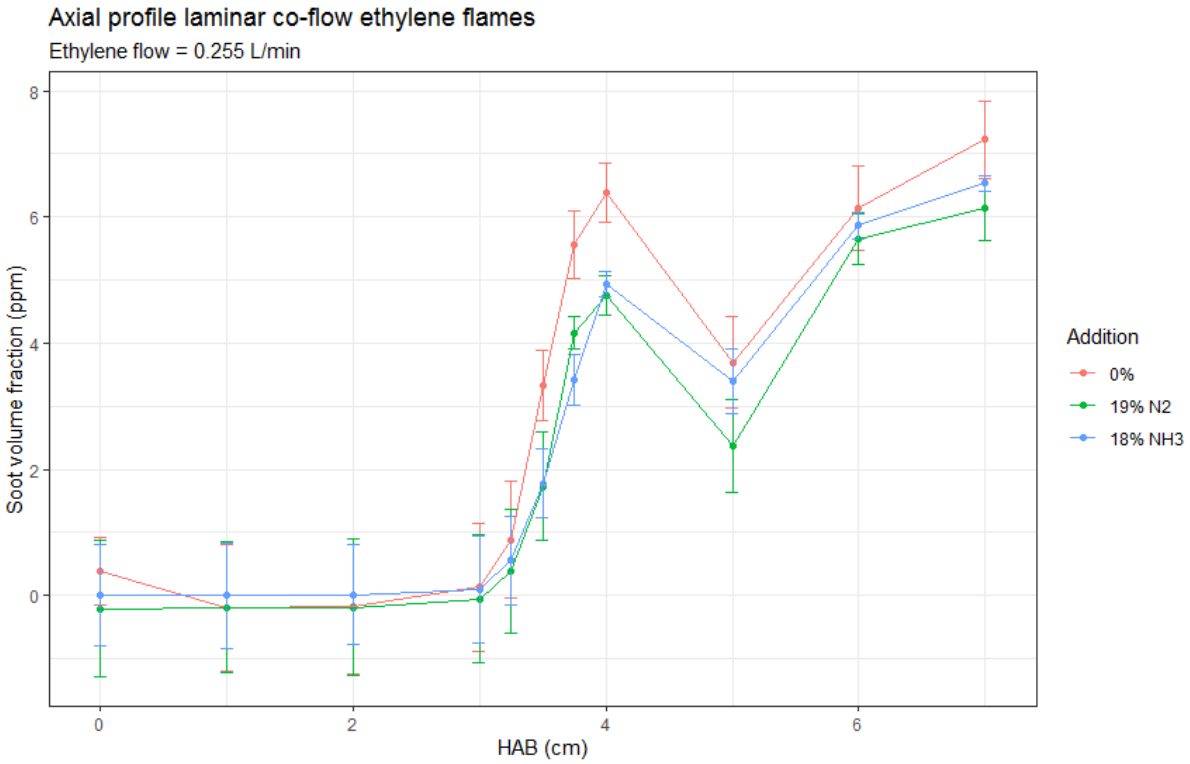

Figure 4-4. Result ethylene SFV measurements with addition at exit velocity 13 cm/s.

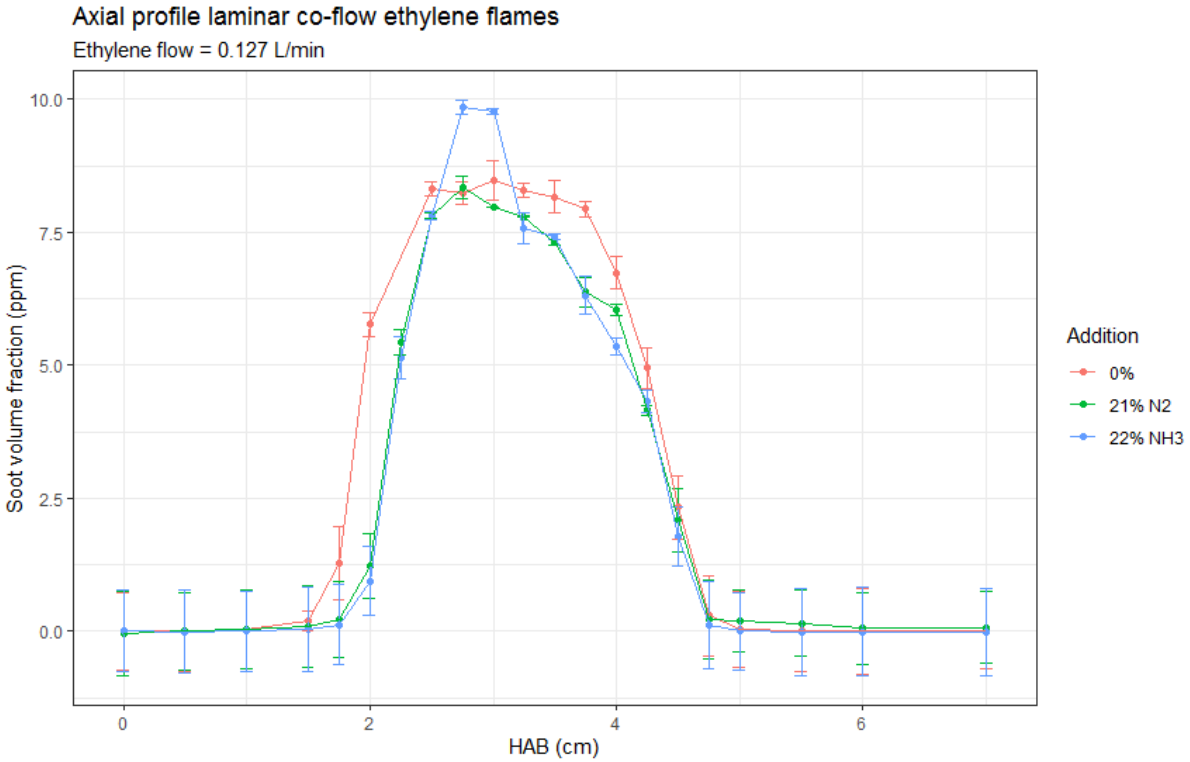

Figure 4-5. Results ethylene SVF with same carbon flow as methane reference flame.

Next, ethylene flow was halved in order to get the same carbon flux as in the methane experiments for a better comparison between the two fuels. This led to a similar flow rate as in Ren et al. (2022). However, no suppressive effect on soot formation was found (figure 4-5). This suggests that the suppressive effect has a volumetric doping percentage threshold. It should be noted that peak SVF in both ethylene experiments were similar. However, in the ethylene experiment with the same carbon flow as the methane reference flame the SVF went down with HAB after reaching a peak around HAB 3cm, whereas in the experiment with the same exit velocity this was not the case. If eventually SVF goes down again could not be measured due to limitations in positioner range. Quantification of SVF did result in similar values reported in literature for both methane and ethylene, indicating a sound calibration.

To further investigate the effects of ammonia addition to carbonaceous fuels, more measurements need to be done. Complementary to suggestions made including varying the doping range and experimenting with other flame characteristics, other measurements can be done. Measurements such as temperature measurements using rapid thermocouple insertion techniques can estimate temperatures without interference from soot particles, which is the case if Raman spectroscopy is used. This in combination with soot sampling for analysis by TEM, as well as an investigation of the exhaust gasses using gas chromatography and mass spectrometry might shed more light on the specific combustion processes. Combining all data will create a better picture and which can then be used to improve or validate kinetic chemical analysis models.
Before ammonia addition to combustion processes is implemented in practice, care should be taken that the reduction in soot formation and possibly carbon dioxide emission is not offset by the increase in NOx production. While interesting, this discussion is outside the scope of this thesis.

5. CONCLUSION

The main research question formulated in the introduction was:

"What is the effect of co-combusting ammonia with carbonaceous fuels of flame soot formation?"

From the experiments, we can conclude that ammonia has a potential suppressive effect on soot formation when co-combusted with carbonaceous fuels. However, the effect depends on the combusted fuel, is observed under specific circumstances, and has a possible threshold before suppression starts. Furthermore, it can be concluded that the suppressive effect in methane flames is mostly chemical in nature, as doping with nitrogen does not suppress soot formation in the same amount as doping with ammonia.

The stated sub question was:

"Does fuel type alter the effect of ammonia addition on soot formation, i.e. is there a difference in the effect between ethylene and methane flames?"

No suppressive effect was observed in ethylene flames, and thus it can be concluded that fuel type significantly alters the effect of ammonia addition on soot formation.

Based on these conclusions, the hypothesis that ammonia supresses soot formation in methane and ethylene flames is partly rejected. Suppression was found in methane flames, but not in ethylene flames.

6. RECOMMENDED FUTURE RESEARCH

In order to get a better insight into ammonia (co-)combustion, more research is needed. Some suggestions for future experiments are given below.

- Investigate a broader range of doping concentrations to assess the proportionality of soot suppression to volumetric addition percentages.
- Performing radial measurements in order to calculate total integrated soot fraction of the flame.
- Performing temperature measurements using rapid thermocouple insertion technique.
- Analysis of gases produced by combustion using gas chromatography and mass spectrometry.
- Analysis of soot morphology by TEM.
- Analysis of ammonia co-combustion in real application scenarios.

7. LITERATURE

Amos, W. A. (1998). *Costs of storing and transporting hydrogen*. National Renewable Energy Laboratory.

Appl, M. (2011). Ammonia, 1. Introduction. *Ullmann's Encyclopedia of Industrial Chemistry* (). Wiley-VCH Verlag GmbH & Co. KGaA. https://doi.org/10.1002/14356007.a02_143.pub3

Bennet, A. M., Liu, P., Li, Z., Kharbatia, N. M., Boyette, W., Masri, A. R., & Roberts, W. L. (2020). Soot formation in laminar flames of ethylene/ammonia. *Combustion and Flame, 220*, 210-218. https://doi.org/10.1016/j.combustflame.2020.06.042

Bockhorn, H., Fetting, F., Meyer, U., Reck, R., & Wannemacher, G. (1981). Measurement of the soot concentration and soot particle sizes in propane oxygen flames. *Symposium (International) on Combustion, 18*(1), 1137-1147. https://doi.org/10.1016/S0082-0784(81)80118-X

Boyette, W. R., Steinmetz, S. A., Guiberti, T. F., Dunn, M. J., Roberts, W. L., & Masri, A. R. (2021). Soot formation in turbulent flames of ethylene/hydrogen/ammonia. *Combustion and Flame, 226*, 315-324. https://doi.org/10.1016/j.combustflame.2020.12.019

Engineering Toolbox. (2003). *Reynolds Number.* https://www.engineeringtoolbox.com/reynolds-number-d_237.html

Havenith, R. W. A., Fowler, P. W., Jenneskens, L. W., & Steiner, E. (2003). Trimerization of Ethyne: Growth and Evolution of Ring Currents in the Formation of the Benzene Ring. *The Journal of Physical Chemistry A, 107*(11), 1867-1871. https://doi.org/10.1021/jp0222907

Hecht, E. (2002). *Optics* (4th ed.). Addison-Wesley.

IPCC. (2013). *Climate Change 2013: The Physical Science Basis. Contribution of Working Group I to the Fifth Assessment Report of the Intergovernmental Panel on Climate Change.* (). Cambridge, United Kingdom and New York, NY, USA: Cambridge University Press. https://www.ipcc.ch/site/assets/uploads/2018/02/WG1AR5_all_final.pdf

Kennedy, I. M. (2007). The health effects of combustion-generated aerosols. *Proceedings of the Combustion Institute, 31*(2), 2757-2770. https://doi.org/10.1016/j.proci.2006.08.116

Kobayashi, H., Hayakawa, A., Kunkuma, K. D., Somarathne, A., & Okafor, E. C. (2019). Science and technology of ammonia combustion. *Proceedings of the Combustion Institute, 37*(1), 109-133. https://doi.org/10.1016/j.proci.2018.09.029

Langenkamp, P. N. (2018). *Laser Diagnostics of Combustion-Generated Nanoparticles*

Liu, Y., Cheng, X., Li, Y., Qiu, L., Wang, X., & Xu, Y. (2021). Effects of ammonia addition on soot formation in ethylene laminar diffusion flames. *Fuel, 292*, 120416. https://doi.org/10.1016/j.fuel.2021.120416

Mahmoud, S., Nathan, G., Alwahabi, Z., Sun, Z., Medwell, P., & Dally, B. (2018). The effect of exit Reynolds number on soot volume fraction in turbulent non-premixed jet flames. *Combustion and Flame, 187*, 42-51. https://doi.org/10.1016/j.combustflame.2017.08.020

Michelsen, H. A., Schulz, C., Smallwood, G. J., & Will, S. (2015). Laser-induced incandescence: Particulate diagnostics for combustion, atmospheric, and industrial applications. *Progress in Energy and Combustion Science, 51*, 2-48. https://doi.org/10.1016/j.pecs.2015.07.001

Montgomery, M. J., Kwon, H., Dreyer, J. A. H., Xuan, Y., McEnally, C. S., & Pfefferle, L. D. (2021). Effect of ammonia addition on suppressing soot formation in methane co-flow diffusion flames. *Proceedings of the Combustion Institute, 38*(2), 2497-2505. https://doi.org/10.1016/j.proci.2020.06.094

Pejpichestakul, W., Ranzi, E., Pelucchi, M., Frassoldati, A., Cuoci, A., Parente, A., & Faravelli, T. (2019). Examination of a soot model in premixed laminar flames at fuel-rich conditions. *Proceedings of the Combustion Institute, 37*(1), 1013-1021. https://doi.org/10.1016/j.proci.2018.06.104

Pöschl, U. (2005). Atmospheric Aerosols: Composition, Transformation, Climate and Health Effects. *Angewandte Chemie (International Ed.), 44*(46), 7520-7540. https://doi.org/10.1002/anie.200501122

Ren, F., Cheng, X., Gao, Z., Huang, Z., & Zhu, L. (2022). Effects of NH3 addition on polycyclic aromatic hydrocarbon and soot formation in C2H4 co-flow diffusion flames. *Combustion and Flame, 241*, 111958. https://doi.org/10.1016/j.combustflame.2021.111958

Rouwenhorst, K. H. R., Krzywda, P. M., Benes, N. E., Mul, G., & Lefferts, L. (2020). Ammonia, 4. Green Ammonia Production. *Ullmann's Encyclopedia of Industrial Chemistry* (). Wiley-VCH Verlag GmbH & Co. KGaA. https://doi.org/10.1002/14356007.w02_w02

Santoro, R. J., & Shaddix, C. R. (2002). Chapter 9: Laser-Induced Incandescence. In K. Kohse-Höinghaus, & J. B. Jeffries (Eds.), *Applied Combustion Diagnostics* (1st ed., pp. 253-286). CRC Press. https://doi.org/10.1201/9781498719414

Sepman, A. V., Mokhov, A. V., & Levinsky, H. B. (2013). Spatial structure and NO formation of a laminar methane–nitrogen jet in hot coflow under MILD conditions: A spontaneous Raman and LIF study. *Fuel, 103*, 705-710. https://doi.org/10.1016/j.fuel.2012.10.010

Shao, C., Campuzano, F., Zhai, Y., Wang, H., Zhang, W., & Sarathy, M. S. (2022). Effects of ammonia addition on soot formation in ethylene laminar premixed flames. *Combustion and Flame, 235*, 111698. https://doi.org/10.1016/j.combustflame.2021.111698

Smyth, K. C., & Shaddix, C. R. (1996). The elusive history of m~= 1.57 – 0.56i for the refractive index of soot. *Combustion and Flame, 107*(3), 314-320. https://doi.org/10.1016/S0010-2180(96)00170-8

Sorensen, C. M. (2001). Light Scattering by Fractal Aggregates: A Review. *Aerosol Science & Technology, 35*(2), 648-687. https://doi.org/10.1080/02786820117868

Steinmetz, S. A., Ahmed, H. A., Boyette, W. R., Dunn, M. J., Roberts, W. L., & Masri, A. R. (2022). Effects of ammonia and hydrogen on the sooting characteristics of laminar coflow flames of ethylene and methane. *Fuel, 307*, 121914. https://doi.org/10.1016/j.fuel.2021.121914

UNFCCC. (2015). *The Paris Agreement*

Valera-Medina, A., Xiao, H., Owen-Jones, M., David, W. I. F., & Bowen, P. J. (2018). Ammonia for power. *Progress in Energy and Combustion Science, 69*, 63-102. https://doi.org/10.1016/j.pecs.2018.07.001

Wang, B., Li, T., Gong, F., Othman, M. H. D., & Xiao, R. (2022). Ammonia as a green energy carrier: Electrochemical synthesis and direct ammonia fuel cell - a comprehensive review. *Fuel Processing Technology, 235*, 107380. https://doi.org/10.1016/j.fuproc.2022.107380

Wang, Y., & Chung, S. H. (2019). Soot formation in laminar counterflow flames. *Progress in Energy and Combustion Science, 74*, 152-238. https://doi.org//10.1016/j.pecs.2019.05.003

Warnatz, J., Maas, U., & Dibble, R. W. (2006). *Combustion: Physical and Chemical Fundamentals, Modeling and Simulation, Experiments, Pollutant Formation* (4th ed.). Springer-Verlag Berlin Heidelberg New York. https://doi.org/10.1007/978-3-540-45363-5

Xi, J., Yang, G., Cai, J., & Gu, Z. (2021). A Review of Recent Research Results on Soot: The Formation of a Kind of Carbon-Based Material in Flames. *Frontiers in Materials, 8*, 695485. https://doi.org/10.3389/fmats.2021.695485

Zhu, X., Khateeb, A. A., Roberts, W. L., & Guiberti, T. F. (2021). Chemiluminescence signature of premixed ammonia-methane-air flames. *Combustion and Flame, 231*, 111508. https://doi.org/10.1016/j.combustflame.2021.111508

8. APPENDICES

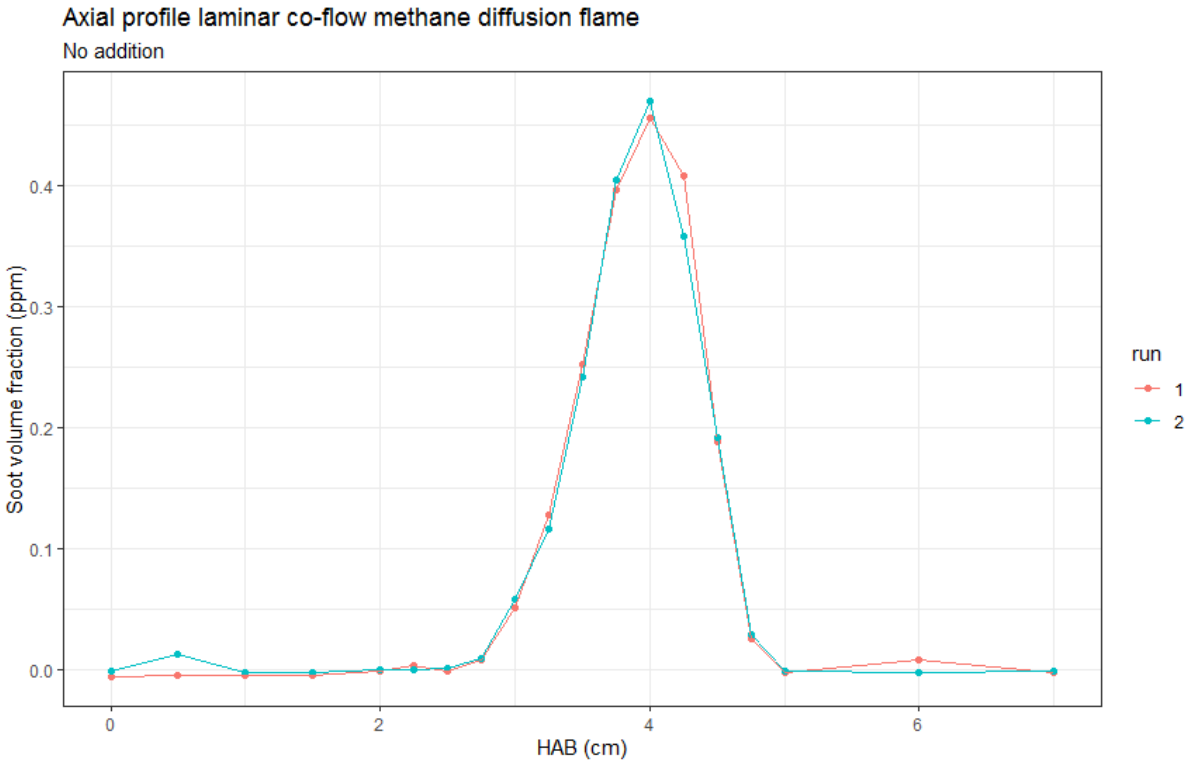

Figure 8-1. Consecutive axial profiles measured of a pure methane co-flow diffusion flame.

Figure 8-2. From left to right, CH_4 + NH_3, CH_4 + N_2, and pure CH_4. CH_4 flow 0,25 L/min.

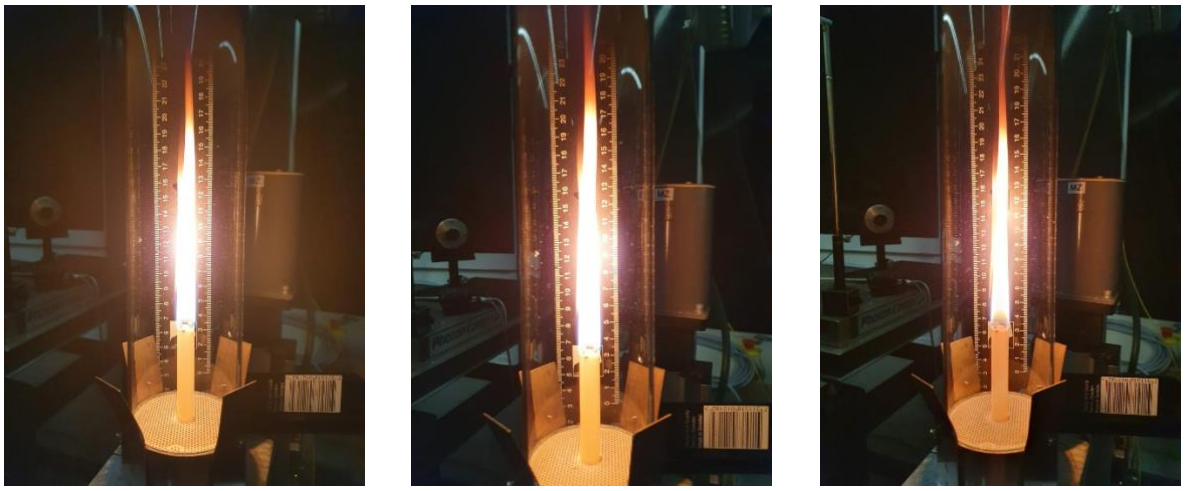

Figure 8-3. From left to right, C_2H_4 + NH_3, C_2H_4 + N_2, and pure C_2H_4. C_2H_4 flow 0,25 L/min.

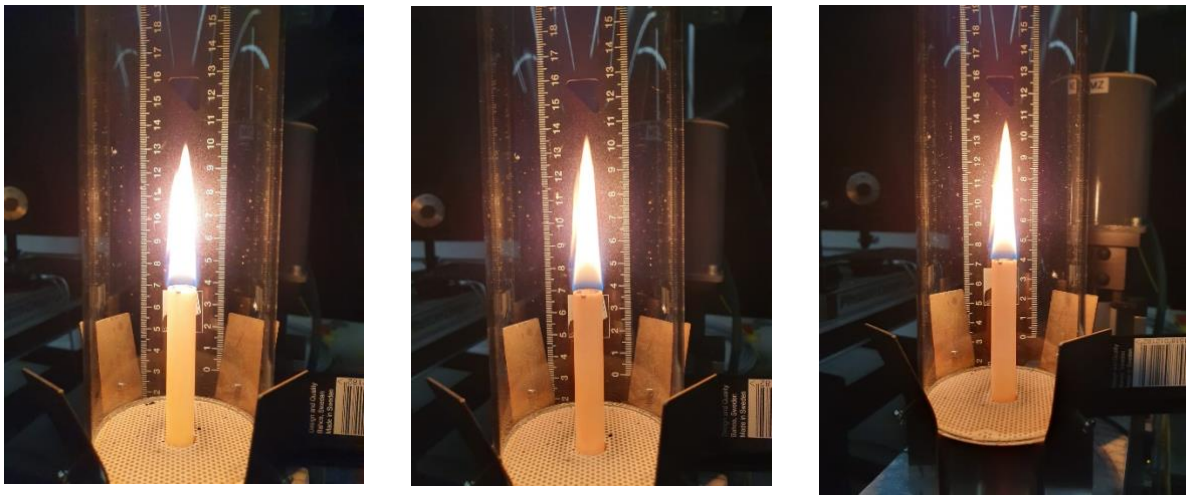

Figure 8-4. From left to right, C2H4 + NH3, C2H4 + N2, and pure C2H4. C2H4 flow 0,12 L/min.